



RESEARCH ARTICLE

Design, structural, and electrical conduction behavior of Zr-modified BaTiO₃-BiFeO₃ perovskite ceramics

Siddharth P. Singh¹, Amar B. Verma¹, Ankur Srivastava¹, Kamlesh K. Chaurasiya², Anil Kumar¹, Prashant K. Singh³, Sindhu Singh^{1*}

Abstract

This study employs the solid-state reaction method to synthesize [(Ba_{0.7}Bi_{0.3})(Ti_{0.7-y}Zr_y)Fe_{0.3}]O₃ (y = 0.0, 0.2, 0.3, 0.4, 0.6) for investigating their structural and DC conduction behavior. XRD analysis suggests a perovskite phase for all the compositions having a cubic crystal structure. Initially, average crystallite size increases for y ≥ 0.3 and then decreases for y = 0.4. The temperature-dependent DC electrical conductivity demonstrated the semiconducting nature for all the compositions. The introduction of Zr modifies the material's structure and electrical properties evident in the observed variations in crystallite size and conductivity behavior. These findings contribute to the understanding of Zr-modified [(Ba_{0.7}Bi_{0.3})(Ti_{0.7-y}Zr_y)Fe_{0.3}]O₃ ceramics, shedding light on their potential applications in semiconductor devices and solid-state electronics. The investigation underscores the importance of tailoring composition parameters for fine-tuning material characteristics, opening avenues for optimized utilization in electronic and energy-related technologies.

Keywords: Solid state ceramic route, Complex perovskites, XRD, DC conductivity.

Introduction

The pursuit of advanced materials with tailored structural and electrical properties has been a driving force behind numerous technological advancements, particularly in electronics, energy storage, and sensing (Krohns *et al.*, 2011; R. E. Cohen, 1992). Among such materials, Barium titanate, i.e., BaTiO₃ (BTO) is a well-established material belonging to

ferroelectric known for its perovskite crystal structure and high dielectric constant. Beyond the Curie temperature, T_c (130°C), the crystal structure of BTO is cubic (space group Pm3m). However, it shows three-phase transitions upon cooling: at temperatures 130, 0, and -90°C corresponding phase transitions are cubic to tetragonal (space group P4mm), tetragonal to orthorhombic (Pmm2), and orthorhombic to rhombohedral (R3C), respectively. A second-order Jahn teller distortion implying orbital hybridization among Ti 3p and O 2p is present in these transitions. Ions of Ti (Ti⁴⁺) can be shifted with respect to anions as a result of this hybridization, which leads to distinct crystallographic orientations and spontaneous polarisation (Battoo *et al.*, 2021; Sreenivas *et al.*, 1987). However, to enhance its ferroelectric performance and stability, various doping methods have been explored. To modify the structural and electrical properties of BTO, zirconium (Zr) doping has emerged as an effective method.

In contrast, bismuth ferrite, (BiFeO₃), (BFO) has gained attention for its multiferroic properties, exhibiting simultaneous ferroelectric and antiferromagnetic ordering at room temperature (Sosnowska *et al.*, 1982). The coexistence of these properties opens up possibilities for coupling between electric and magnetic fields, enabling novel functionalities such as electric field control of magnetism. However, BFO has limitations, such as low magnetic saturation and coercive field, which hinder its practical applications (Neaton *et al.*, 2005; Wu *et al.*, 2016). To address these challenges, doping

¹Material Synthesis Laboratory, Department of Physics and Electronics, Dr. Rammanohar Lohia Avadh University, Ayodhya, Uttar Pradesh, India

²Department of Physics, Rajkiya P.G. College Musafirkhana, Amethi, Uttar Pradesh, India

³Department of Applied Sciences and Humanities, Institute of Engineering and Technology, Dr. Rammanohar Lohia Avadh University, Ayodhya, Uttar Pradesh, India

***Corresponding Author:** Sindhu Singh, Material Synthesis Laboratory, Department of Physics and Electronics, Dr. Rammanohar Lohia Avadh University, Ayodhya, Uttar Pradesh, India, E-Mail: sindhusingh@rmlau.ac.in

How to cite this article: Singh, S. P., Verma, A. B., Srivastava, A., Chaurasiya, K. K., Kumar, A., Singh, P. K., Singh, S. (2024). Design, structural, and electrical conduction behavior of Zr-modified BaTiO₃-BiFeO₃ perovskite ceramics. *The Scientific Temper*, 15(2):2045-2049.

Doi: 10.58414/SCIENTIFICTEMPER.2024.15.2.12

Source of support: Nil

Conflict of interest: None.

strategies have been employed to tailor the structural and magnetic properties of BFO. Zr doping, in particular, has been shown to enhance the magnetic properties of BFO by manipulating the magnetic interactions and spin structures within the material (Shen *et al.*, 2016). Investigation of structural modifications induced by Zr doping in BFO is essential for optimizing its magnetic behavior and harnessing its potential for applications in spintronic devices, magnetic data storage, and magnetoelectric devices (Mahesh Kumar, Suresh *et al.*, 1998).

In this research article, we present a comprehensive investigation into the structural and electrical properties of $[(\text{Ba}_{0.7}\text{Bi}_{0.3})(\text{Ti}_{0.7-y}\text{Zr}_y)\text{Fe}_{0.3}]\text{O}_3$ ($y=0.0, 0.2, 0.3, 0.4, 0.6$) systems. Through XRD and DC conductivity measurements, we aim to elucidate the effects of Zr doping on the crystal structure and electrical conductivity behavior of these materials. By understanding the interplay between structural defects, charge carriers, and conduction mechanisms, we seek to advance the design of multifunctional materials for future electronic and energy-related applications.

Materials and Methodology

Figure 1 represents the preparation of $[(\text{Ba}_{0.7}\text{Bi}_{0.3})(\text{Ti}_{0.7-y}\text{Zr}_y)\text{Fe}_{0.3}]\text{O}_3$ ($y=0.0, 0.2, 0.3, 0.4, 0.6$) ceramics by the method of solid-state reaction. Analytical reagent grades BaCO_3 , Bi_2O_3 , TiO_2 , ZrO_2 , and Fe_2O_3 , with a purity level of 99.99%, were used as raw materials for the perovskite ceramics. The stoichiometric proportions for various compositions were weighed and mixed using an agate mortar pestle for 6 hours. This method involves atomic-level mixing between the precursors. The smaller the particle size, the greater will be the ratio of surface area to volume. Since surfaces are higher energy regions, they will constantly try to reduce their area and thus lower their energy when possible, which will result in lower calcination temperature. Furthermore,

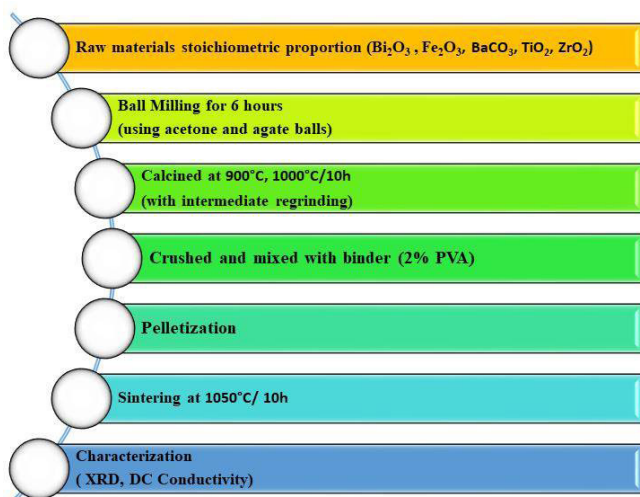


Figure 1: Flow chart representing preparation of samples using solid-state reaction route

the difference in particle size between the precursors used may also accelerate the calcination reaction and lower the processing temperature (Patel *et al.*, 2011). The mixed compositions were dried and calcined progressively at $900^\circ\text{C}/10\text{h}$ and $1000^\circ\text{C}/10\text{h}$, respectively. The calcined powder was again mixed with 2% PVA. The mixture was then pressed into a single bulk pellet through a stainless-steel die of diameter 12 mm and a thickness of 2 mm by applying a pressure of 60 N/m^2 using a hydraulic press. The green samples were kept on an alumina lid for sintering at $1050^\circ\text{C}/10\text{h}$. A few sintered pellets were crushed into fine powder for structural analysis, while other pellets were used for electrical experiments. Single-phase check and structural formation for the material were carried out using an X-ray powder diffractometer, PANalytical X'Pert Pro, with CuK_α radiation ($\lambda = 1.540\text{ \AA}$) at ambient temperature. The DC conductivity was measured in the temperature range of $27\text{--}447^\circ\text{C}$ using a Keithley 224 Programmable Current Source and KEYSIGHT 34465A $6_{1/2}$ Digit Multimeter.

Results and Discussion

XRD Analysis

The X-ray pattern obtained at RT for the compositions $[(\text{Ba}_{0.7}\text{Bi}_{0.3})(\text{Ti}_{0.7-y}\text{Zr}_y)\text{Fe}_{0.3}]\text{O}_3$ ($y=0.0, 0.2, 0.3, 0.4, 0.6$) are given in Figure 2. The XRD results show the single-phase formation. For the compositions $y=0.0, 0.2, 0.3, 0.4$, all the XRD peaks could be matched with the ideal cubic structure (Pm-3m space group, JCPDS card no: 98-001-0445 without any secondary phase. The existence of an extra peak indicates that a single phase is not formed for $y=0.6$. From Figure 2, it can be observed that as the doped Zr amount is increased, a shift in the diffraction peak towards lower 2θ is observed,

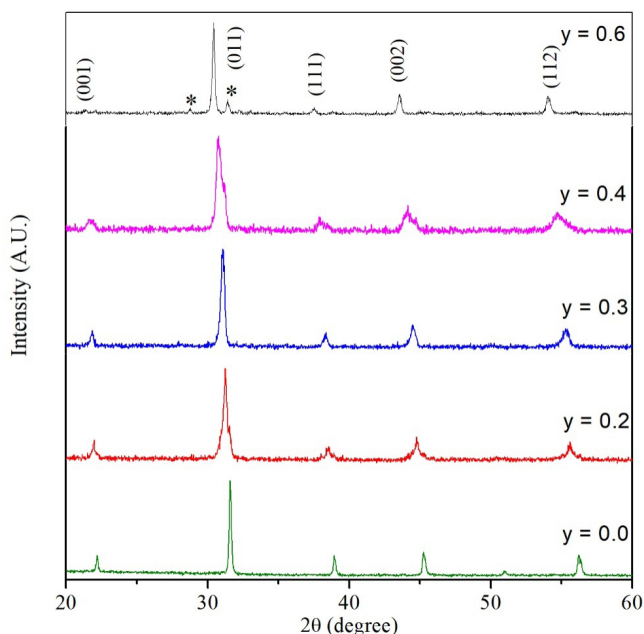


Figure 2: XRD pattern of Zr doped BaTiO_3 - BiFeO_3 compounds

Table 1: Lattice parameters and related properties

Parameters	0%	0.2%	0.3%	0.4%
Lattice constants (Å)	4.004835	4.044353	4.064151	4.10710
Cell volume (Å ³)	64.232	66.153	67.129	69.2798
X-ray density (g/cm ³)	6.64	6.66	6.68	6.57
Bulk density (g/cm ³)	6.18	6.15	5.08	5.88
Porosity (%)	6.92	7.65	5.08	10.50
Crystallite size (D) (nm)	460.49	523.22	597.64	298.82

similar to the results reported for Zr⁴⁺ doping (Jha *et al.*, 2014). Analysis reveals an increase in lattice parameters because of doping. As Zr⁴⁺ ions (0.72Å) may enter into the B-site and replace the Ti⁴⁺ ions (0.605Å), consequently, an increase in the lattice parameters with increasing doping concentration of Zr (Zhang *et al.*, 2022). Change in the shape of a peak for y = 0.4 indicates the occurrence of structural distortion or transformation.

Crystallite size (D) was calculated using the Debye-Scherrer equation (Anupama *et al.*, 2017; Batoo *et al.*, 2021):

$$D = \frac{k\lambda}{\beta \cos\theta} \quad (1)$$

Where k denotes the structure factor and has a value 0.9 or 1 for the cubic system, $\lambda = 1.54 \text{ \AA}$ represents a wavelength of Cu-K_α radiation, β represents full-width half maxima (FWHM), θ denotes Bragg's angle. β and θ both are taken in radians.

Table 1 tabulates lattice constant, cell volume, X-ray density, bulk density, porosity, and crystallite size for studied compositions. From Table 1, it can be observed that crystallite size shows an increase from 460.49 to 597.64 nm for $y \geq 0.3$. Further, it reduces to 298.82 nm for $y = 0.4$. As reported in earlier studies, the formation of oxygen vacancies can reduce the crystallite size (Chchiyai *et al.*, 2021). Therefore, an increase in oxygen vacancies may explain the crystallite size decreases for $y = 0.4$.

Theoretical density was calculated using the following relation (R. Verma *et al.*, 2021):

$$\rho_{th} = \frac{Z.M}{N.V} \quad (2)$$

Here, Z represents the number of molecules per unit cell (1 for perovskite) (Coondoo *et al.*, 2018), M represents molecular weight, V represents volume and N shows Avogadro's number.

The density (experimental) for all the samples was determined using the following relation (V. Verma *et al.*, 2008):

$$\rho_{exp} = \frac{m}{V} = \frac{m}{\pi r^2 h} \quad (3)$$

Where m is the mass of the pellet, V shows the volume, r shows the radius of the pellet, and h shows the thickness of the cylindrical pellets. We have determined the percentage porosity by the following relation (Farea *et al.*, 2009):

$$\%Porosity = \left(1 - \frac{\rho_{exp}}{\rho_{th}}\right) \times 100 \quad (4)$$

The theoretical density increases with the doping of Zr⁴⁺ ion at Ti –site from $y = 0.0$ to $y = 0.3$ on the other hand, with further increase in doping of Zr⁴⁺ ion, it decreases for $y = 0.4$. This could be because of donor doping, which produces oxygen and cation vacancies to preserve charge neutrality. The oxide system that consists of oxygen vacancies encourages mass transport during sintering, resulting in denser grains (Batoo *et al.*, 2021).

Porosity fluctuation may be correlated with the presence of a particle size distribution, i.e., smaller the particle size, lower the porosity, and vice-versa (Yan *et al.*, 2011). Therefore, the rise in porosity with an increase in Zr⁴⁺ ion shows an increase in particle size. Thus, variation in theoretical density and porosity shows that with the increase in Zr ion in the BTO-BFO lattice, particle size increases.

DC Conduction Properties

The plots of DC conductivity *versus* temperature for Zr-doped BTO-BFO ceramics are shown in Figure 3.

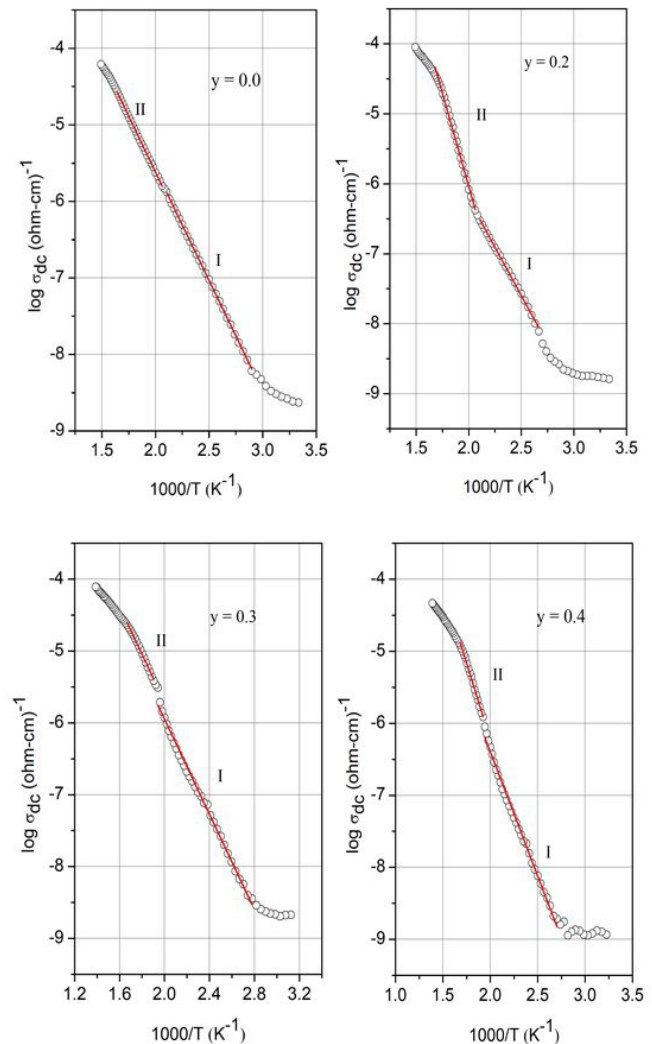


Figure 3: Temperature-dependent DC conductivity graph for compositions: $y = 0.0$, $y = 0.2$, $y = 0.3$ and $y = 0.4$.

Table 2: Activation energy, E_a for DC conduction in the system $[(\text{Ba}_{0.7}\text{Bi}_{0.3})(\text{Ti}_{0.7-y}\text{Zr}_y)\text{Fe}_{0.3}]\text{O}_3$

Composition	Temperature range (°C)	E_a (eV)
y = 0.0	72–202	0.57
	207–337	0.58
y = 0.2	102–202	0.54
	207–317	1.11
y = 0.3	87–242	0.657
	247–327	0.659
y = 0.4	97–242	0.68
	247–322	0.84

All the compounds show negative temperature coefficients of resistance, i.e., the resistance decreases when temperature increases. For all the compounds, i.e., $y = 0.0-0.4$, plots show two linear regions in the temperature range of 27 to 447°C, which indicates that DC conductivity follows the Arrhenius behavior. The activation energy (E_a) obtained by least square data fitting at various temperature ranges is given in Table 2. In all the compounds, the value of E_a increases with an increase in temperature. The obtained activation energies (E_a) lie in the same range as reported in the previous literature (0.8–1.1 eV) (Mahesh Kumar, Srinivas, *et al.*, 1998). The conductivity value for Zr doped compound is considerably less at RT ($1.16 \times 10^{-9} \Omega^{-1}\text{cm}^{-1}$) when compared to undoped BTO-BFO ($2.35 \times 10^{-9} \Omega^{-1}\text{cm}^{-1}$). Impurity conduction may be the cause of the initial slope change (Mahesh Kumar, Suresh, *et al.*, 1998).

Conclusion

In the present work, the multiferroic compounds with compositions $y = 0.0-0.6$ in the system $(1-x)$ BTO – (x) BFO were synthesized and studied for structural and electrical properties. Room temperature XRD reveals the formation of a single-phase solid solution. XRD analysis reveals the cubic structure for the compositions ($y = 0.0, 0.2, 0.3$ and 0.4). The measurement of temperature dependent DC conductivity showed that studied ceramics are semiconductor in nature. Thus, studying the above material and enhancement in its electrical properties finds a base for device engineering. This could include investigating new materials with unique electronic properties, such as 2D materials like graphene.

Acknowledgment

This work was funded by the Uttar Pradesh government under the Research and Development scheme Grant no. – 80/2021/1543/sattar-4-2021-4(28)/2021.

References

Anupama, M. K., Rudraswamy, B., & Dhananjaya, N. (2017). Investigation on impedance response and dielectric relaxation of Ni-Zn ferrites prepared by self-combustion technique. *Journal of Alloys and Compounds*, 706, 554–561.

- Batoo, K. M., Verma, R., Chauhan, A., Kumar, R., Hadi, M., Aldossary, O. M., & Douri, Y. Al. (2021). Improved room temperature dielectric properties of Gd³⁺ and Nb⁵⁺ co-doped Barium Titanate ceramics. *Journal of Alloys and Compounds*, 883, 160836.
- Chchiyai, Z., El Bachraoui, F., Tamraoui, Y., Haily, E. M., Bih, L., Lahmar, A., Alami, J., & Manoun, B. (2021). Design, structural evolution, optical, electrical and dielectric properties of perovskite ceramics $\text{Ba}_{1-x}\text{Bi}_x\text{Ti}_{1-x}\text{Fe}_x\text{O}_3$ ($0 \leq x \leq 0.8$). *Materials Chemistry and Physics*, 273(June).
- Coondoo, I., Panwar, N., Alikin, D., Bdikin, I., Islam, S. S., Turygin, A., Shur, V. Y., & Kholkin, A. L. (2018). A comparative study of structural and electrical properties in lead-free BCZT ceramics: Influence of the synthesis method. *Acta Materialia*, 155, 331–342.
- Farea, A. M. M., Kumar, S., Batoo, K. M., Yousef, A., Lee, C. G., & Alimuddin. (2009). Influence of the doping of Ti⁴⁺ ions on electrical and magnetic properties of $\text{Mn}_{1+x}\text{Fe}_{2-2x}\text{Ti}_x\text{O}_4$ ferrite. *Journal of Alloys and Compounds*, 469(1–2), 451–457.
- Jha, P. A., Jha, P. K., Jha, A. K., Kotnala, R. K., & Dwivedi, R. K. (2014). Phase transformation and two-mode phonon behavior of $(1-x)[\text{BaZr}_{0.025}\text{Ti}_{0.975}\text{O}_3]-(x)[\text{BiFeO}_3]$ solid solutions. *Journal of Alloys and Compounds*, 600, 186–192.
- Krohns, S., Lunkenheimer, P., Meissner, S., Reller, A., Gleich, B., Rathgeber, A., Gaugler, T., Buhl, H. U., Sinclair, D. C., & Loidl, A. (2011). The route to resource-efficient novel materials. *Nature Materials*, 10(12), 899–901.
- Mahesh Kumar, M., Srinivas, A., Suryanarayana, S. V., & Bhimasankaram, T. (1998). Dielectric and impedance studies on BiFeO_3 - BaTiO_3 solid solutions. *Physica Status Solidi (A) Applied Research*, 165(1), 317–326.
- Mahesh Kumar, M., Suresh, M. B., Suryanarayana, S. V., Kumar, G. S., & Bhimasankaram, T. (1998). Dielectric relaxation in $\text{Ba}_{0.96}\text{Bi}_{0.04}\text{Ti}_{0.96}\text{Fe}_{0.04}\text{O}_3$. *Journal of Applied Physics*, 84(12), 6811–6814.
- Patel, R. K., Prakash, C., & Kumar, P. (2011). *Characterizations of BT Ceramics Synthesized by Modified Solid State Route*. *Characterizations of BT Ceramics Synthesized by Modified*, 116, 10–15.
- Neaton, J. B., Ederer, C., Waghmare, U. V., Spaldin, N. A., & Rabe, K. M. (2005). First-principles study of spontaneous polarization in multiferroic BiFeO_3 . *Physical Review B - Condensed Matter and Materials Physics*, 71(1), 1–8.
- R. E. Cohen. (1992). Origin of ferroelectricity in perovskite oxides. *Nature*, 359(July), 136–138.
- Shen, J., Cong, J., Chai, Y., Shang, D., Shen, S., Zhai, K., Tian, Y., & Sun, Y. (2016). Nonvolatile Memory Based on Nonlinear Magnetoelectric Effects. *Physical Review Applied*, 6(2), 1–5.
- Sosnowska, I., Neumaier, T. P., & Steichele, E. (1982). Spiral magnetic ordering in bismuth ferrite. *Journal of Physics C: Solid State Physics*, 15(23), 4835–4846.
- Sreenivas, K., Mansingh, A., & Sayer, M. (1987). Structural and electrical properties of rf-sputtered amorphous barium titanate thin films. *Journal of Applied Physics*, 62(11), 4475–4481.
- Verma, R., Chauhan, A., Neha, Batoo, K. M., Kumar, R., Hadhi, M., & Raslan, E. H. (2021). Effect of calcination temperature on structural and morphological properties of bismuth ferrite nanoparticles. *Ceramics International*, 47(3), 3680–3691.
- Verma, V., Kotnala, R. K., Pandey, V., Kothari, P. C., Radhapiyari, L., & Matheru, B. S. (2008). The effect on dielectric losses in lithium ferrite by cerium substitution. *Journal of Alloys and*

Compounds, 466(1–2), 404–407.

- Wu, J., Fan, Z., Xiao, D., Zhu, J., & Wang, J. (2016). Multiferroic bismuth ferrite-based materials for multifunctional applications: Ceramic bulks, thin films and nanostructures. *Progress in Materials Science*, 84, 335–402.
- Yan, W., Li, N., Li, Y., Liu, G., Han, B., & Xu, J. (2011). Effect of particle size on microstructure and strength of porous spinel

ceramics prepared by pore-forming in situ technique. *Bulletin of Materials Science*, 34(5), 1109–1112.

- Zhang, Y., Huang, R., Zhang, F., Liang, Z., Xie, T., Lin, H. T., & Dai, Y. (2022). Enhancement of piezoelectric properties of BF–BT ceramics by using ZrO₂ powder bed during the sintering process. *Journal of the American Ceramic Society*, November 2022, 2384–2392.